Research Square

Preprints are preliminary reports that have not undergone peer review.
They should not be considered conclusive, used to inform clinical practice,
or referenced by the media as validated information.

Virtual screening to investigate the potential targets and mechanisms of action of "Astragalus-Ligustrum" drug pair in the treatment of non-small cell lung cancer

Zhengting Deng
Taizhou Hospital, Nanjing University of Chinese Medicine
Hu Tian
Taizhou Hospital, Nanjing University of Chinese Medicine
Yuanhua Ding
Taizhou Hospital, Nanjing University of Chinese Medicine
Qiming Jin
Taizhou Hospital, Nanjing University of Chinese Medicine
Yichen Liu
Nanjing University of Chinese Medicine
Tao Liu
liutao@njucm.edu.cn
Nanjing University of Chinese Medicine
Tong Zhao
Shen Chun-ti Nation-Famous Experts Studio for Traditional Chinese Medicine Inheritance Changzhou TCM Hospital, Nanjing University of Chinese Medicine

Research Article

Keywords: virtual screening, Astragalus, Ligustrum, PD-L1, NSCLC

Posted Date: September 20th, 2023

DOI: https://doi.org/10.21203/rs.3.rs-3349225/v1

License: This work is licensed under a Creative Commons Attribution 4.0 International License. Read Full License

Additional Declarations: No competing interests reported.

Abstract

Astragalus membranaceus and Ligustrum lucidum are the common main components in Chinese patent medicine preparations which have been widely used in combination chemotherapy for tumor treatment. However, the specific mechanism of their anti-cancer effect has not been fully elucidated, and the traditional monomer research mode can hardly reflect the feature of Chinese medicine in treating diseases. In this study, virtual screening was used to explore the mechanism of “Astragalus-Ligustrum” drug pair in the treatment of non-small cell lung cancer (NSCLC). 28 active ingredients and 180 active ingredient targets were screened out from the drug pair by network pharmacology. Among them, 10 components, including quercetin and kaempferol, are the main active ingredients in the drug pair, whose mechanism of anti-NSCLC is to modulate the pathways of PI3K-Akt, PD-1/PD-L1, and T-cell receptor, and by affecting the biological processes such as protein phosphorylation and cellular response to growth factor stimulation. Then molecular docking and molecular dynamics validation showed that the complexes can bind tightly to target proteins in the active pocket through van der Waals, hydrophobic and π-bonds. The binding of PD-L1 to the main active ingredient may be one of the important mechanisms of its anti-NSCLC action. At last, Survival curve analysis and immunohistochemical analysis showed TP53, PIK3R1, PD-L1 and other target genes above had significant differences in expression in lung cancer patients. In conclusion, this study explored the active components of "Astragalus-Ligustrum" drug pair in anti-NSCLC and elucidated the mechanism of its action.

Highlights

1. Quercetin, kaempferol, isorhamnetin, huperzine, astragaloside and other 10 components were identified as the main active ingredients of "Astragalus-Ligustrum" drug pair for its anti-NSCLC treatment.

2. All the active ingredients except for huperzine had strong binding activity with AKT1 and PD-L1.

3.The binding activity between PD-L1 and the main active ingredient might be one of the important mechanisms.

1. Introduction

Lung cancer is one of the common malignant tumors in the world. Its incidence and mortality rates are high over the few decades, and the 5-year survival rate is only 21.7%.[1] According to histopathological characteristics, lung cancer can be divided into non-small cell lung cancer (NSCLC) and small cell lung cancer (SCLC), of which NSCLC accounts for about 80–85% of all.[2] The clinical symptoms of NSCLC patients are not obvious or asymptomatic in the early stage of the disease, which is highly insidious. As the condition progresses, symptoms such as low fever, cough, and difficulty breathing gradually appear, which greatly affects the patient's life and safety.[3] Currently, surgery is the most desirable treatment for these patients.[4] Although minimally invasive techniques have achieved greater results in recent years, the results of surgery alone are still not optimistic, especially in the N2 stage, where the local recurrence rate and distant metastasis rate can be as high as 20% and 50% or even more, respectively. The suitability of surgical treatment for patients with intermediate to advanced disease is still debatable. Currently, the preferred treatment still relies on medical drug therapy such as chemotherapy, radiotherapy, immunotherapy, and targeted therapy, but it is often accompanied by many adverse effects such as bone marrow suppression, gastrointestinal reactions, and liver and kidney function impairment due to different patient tolerance. In addition to improving the quality and prolonging the survival of patients, an increasing number of studies have found Chinese medicine as an adjuvant therapy to enhance the effect of internal medicine treatment and reduce the related adverse effects. [5]

A series of studies has found that immunosuppression of tumor microenvironment is an intrinsic factor in the development of tumor, and tumor immunotherapy can stimulate and enhance the immune function of the body to

control and kill tumor cells.[6] According to traditional Chinese medicine theory, tonic Chinese medicine has become an important and indispensable part of lung cancer treatment because of its characteristics of increasing the immune function of the body, improving microcirculation, reducing clinical symptoms and prolonging survival time with tumor.[6] Astragalus is the dried root of Astragalus mongolica or Astragalus membranaceus, a legume.[7] Ligustrum is the fruit of Chaste Tree, a plant of the family Lignanaceae, both of which are common tonic Chinese medicines[8]. It has obvious anti-cancer effects on tumor cell growth and metastasis of stomach, colon, breast, lung, mammary gland, and can regulate the immune function of cancer patients. Chinese patent medicine preparations of Ligustrum lucidum and Astragalus membranaceus as the main components (such as Zhenqi Fuzheng capsule, Zhenqi Fuzheng granule and Zhenqi Fuzheng dispersible tablet) have been widely used in combination chemotherapy for tumor treatment.[9] However, the specific mechanism of their anti-cancer mechanism has not been fully elucidated, and because of the multi-component and multi-target integrated regulation of traditional Chinese medicine in treating diseases, the traditional monomer research mode can hardly reflect this feature of Chinese medicine in treating diseases. The development of modern bioinformatics and systems pharmacology elaborated the special synergistic interactions among the herbs of Chinese medicine formulations through a multi-target and multi-pathway approach. In which network pharmacology exploit the pharmacological mechanism of drug action in the biological network, analyzes the drug's interaction with specific nodes or modules in this network, and explores the drug target from a holistic perspective. Molecular docking can help in the prediction of the binding conformation and binding mode or orientation between a receptor and a ligand and is especially valuable for studying changes of substrate conformation during the formation of Chinese medicine complexes.

Therefore, in this study, network pharmacology was used to screen the active ingredients of "*Astragalus-Ligustrum*" drug pair through relevant databases, and matched their targets with the disease targets of cancer to screen out the potential key targets of its anticancer therapy. The drug-component-target network and key target protein network were constructed and molecular dynamics validated, with the aim of providing a comprehensive understanding of the mechanism of "*Astragalus-Ligustrum*" drug pair against cancer in a systematic manner. The protocol of our study procedures is shown in Fig. 1.

2. Materials and Methods

2.1 Screening of active ingredients and targets in the "*Astragalus-Ligustrum*" drug pair

Use Traditional Chinese Medicine Systems Pharmacology Database and Analysis Platform (TCMSP) [10],https://old.tcmspe.com/tcmsp.php)to collect all chemical components of Astragalus and Ligustrum. Absorption, Distribution, Metabolism and Excretion (ADME) studies are designed to investigate how Chinese medicine can reach the target organs and exert their effects. Among those, oral bioavailability (OB) ≥ 30% and drug likeness (DL) can be used as a screening condition for potentially active constituents. Through PubChem database [11], The TCMSP target data were supplemented by downloading the structural formulae of the components through the PubChem database and then importing them into the Swiss Target Prediction database [12] (http://www.swisstargetprediction.ch/) for further target prediction. Subsequently, the targets were imported into the Uniprot database [13] (https://www.uniprot.org/), with the species restricted to "Human", to normalize the protein target information.

2.2 Screening of NSCLC disease-related targets

Using "non-small cell lung cancer" and "NSCLC" as search terms, we mined the Genecards database [14] (https://www.genecards.org/), OMIM database (Online Mendelian Inheritance in Man, OMIM) [15] (https://omim.org/)

for potential targets for NSCLC. This is supplemented by the Drugbank [16] (https://go.drugbank.com/) collection of clinical first-line Western drug targets for NSCLC. After merging the above disease database targets, duplicate values were removed to obtain the relevant targets for NSCLC.

2.3 Access to active ingredients and common targets in NSCLC by "*Astragalus-Ligustrum*" drug pair

In order to clarify the interaction between the relevant targets of the "*Astragalus-Ligustrum*" drug pair and the targets of NSCLC, a Venn diagram of "disease targets" and "component targets" was created by using the online program Venny 2.1.0 (https://bioinfogp.cnb.csic.es/tools/venny/index.html).The intersection of the two sets of targets was used to identify their common targets, and then using Cytoscape 3.8.2 software to construct a "drug-target-disease" visualisation network.

2.4 Construction and analysis of protein-protein interaction network (PPI)

The common targets were imported into the online String database [17] (https://string-db.org/). “Organism” was set to "Homo sapiens", single node was removed in the network, the minimum interaction threshold was set to "highest confidence (> 0.900). The minimum interaction threshold was set to "highest confidence (> 0.900)", and other parameters were kept as default values to construct the PPI network graph. The network topology parameters were analysed by importing the relevant information into Cytoscape 3.8.2 software and filtered according to the indicators of Degree, Betweenness and Closeness to obtain the core targets of Astragalus- Ligustrum drug for the treatment of NSCLC and its efficacy. The core targets and the main active ingredients of the drug were identified.

2.5 Gene Ontology (GO) and Kyoto Encyclopedia of Genes and Genomes (KEGG)

Pathway enrichment analysis was performed using the Metascape platform[18] (http://metascape.org/gp/index.html) for GO and KEGG enrichment of key targets. Bar graphs were plotted against the enriched gene counts. Take the top 10 entries in GO for biological process (BP), cellular component (CC) and molecular function (MF) and the top 10 entries in KEGG to visualize. Based on this study, the biological process and key signaling pathways of the "*Astragalus-Ligustrum*" drug pair in the treatment of NSCLC were investigated.

2.6 Molecular docking forecasts

The main active ingredient in the "active ingredient-target-pathway" network was selected for molecular alignment with the core target to verify the reliability of the network analysis. A 3D structure of the ligand active ingredient in SDF format was downloaded from the PubChem database and the mol2 file was exported using ChemBio 3D Ultr a 14.0 file. The 3D structures of the targets were searched for from the RCSB Protein Data Bank (PDB, https://www.rcsb.org/) [19] and saved in pdb format. PyMOL software (www.pymol.org) was used to dehydrate the 3D structure of the protein in the PDB download file, and then AutoDockTools-1.5.6 software was used to dehydrate and hydrogenate the active ingredient and target protein, and convert both the active ingredient and target protein file formats to pdb format. Molecular docking was carried out using Auto Dock Vina software (https://vina.scripps.edu/) to investigate the binding interaction between the components and the target site. After docking, the binding energy was used as a reference for screening the active compounds and the affinity ≤ -5.0 kJ/mol was used as the basis for screening the active ingredient targets of the “*Astragalus-Ligustrum*” drug pair [20].

2.7 Molecular dynamics simulations

MD simulations were performed using the Gromacs 2018.4 program [21] at constant temperature and pressure as well as periodic boundary conditions. The Amber14SB all-atom force field [22] and the TIP3P water model [23]were applied. During the MD simulations, all bonds involving hydrogen atoms were constrained using the LINCS algorithm [24]with an integration step of 2 fs. Electrostatic interactions were calculated using the (Particle-mesh Ewald) PME method [25]. The non-bonded interaction truncation value was set to 10 Å and updated every 10 steps. The simulation temperature was controlled by the V-rescale temperature coupling method at 298.15 K [26] and the pressure was controlled by the Parrinello-Rahman method [27] at 1 bar. The steepest descent method was used to minimize the energy of the two systems to eliminate too close contact between the atoms. Then, 1 ns of the 298.15 K condition was used for the NVT and NPT equilibrium simulations were then performed at 298.15 K. Finally, 100 ns MD simulations were performed for the system and the conformation was saved every 10 ps. The visualization of the simulation results was done using the Gromacs embedded program and VMD.

2.8 Survival analysis of key target genes

The Kaplan-Meier Plotter database (https://kmplot.com/analysis/)was used to assess the relationship between target genes and the prognosis of patients with non-small cell lung cancer [28]. A survival analysis of the gene in lung cancer survival prognosis was obtained by entering the name of the core target in the "GENE Symbol", and $P < 0.05$ was considered to be significantly associated with patient survival. Further in-depth identification of non-small cell lung cancer and normal human gene levels using the GEPIA2 online database[29] (http://gepia2.cancer-pku.cn/) yielded a result of $P < 0.05$ suggesting that this gene is a prognostic target for non-small cell lung cancer, suggesting a relationship between this gene and patient prognosis.

2.9 Immunohistochemical analysis

Immunohistochemistry is the localization, characterization as well as quantitative detection of the corresponding antigen or antibody by means of antigen-antibody reactions and tissue chromogenic reactions in tissue cells in situ with the help of markers. The Human Protein Atlas (HPA) database[30] (https://www.proteinatlas.org/) was used to analyze the protein expression of intersectional targets in normal and lung cancer tissues. The differences in protein expression in normal and tumor tissues were compared according to the intensity of protein staining in the tissues and the percentage of stained cells.

3. Result

3.1 Acquisition of active ingredients and targets

The active ingredients of *Astragalus-Ligustrum* (botanical names were checked with http://www.theplantlist.org) were obtained in the TCMSP database according to the screening criteria (OB ≥ 30%, DL ≥ 0.18). Among them, 17 active ingredients of Astragalus and 13 active ingredients of ligustrum were obtained according to the screening criteria (OB ≥ 30%, DL ≥ 0.18), as shown in Table 1. There were two active ingredients of Astragalus and Ligustrum, Quercetin and Kaempferol, respectively. The target proteins corresponding to each active ingredient screened according to the above criteria were obtained from the database, and the TCMSP target data were supplemented by target prediction from PubChem database and Swiss Target Prediction database. Finally, the Uniprot protein database was used to standardize the protein target information, and the corresponding targets of "*Astragalus-Ligustrum*" were identified. At last, the Uniprot protein database was used to standardize the protein target information, and a total of 570 targets were identified for "Astragalus" and " Ligustrum "

Table 1
The Active Ingredient Information of "*Astragalus–Ligustrum* " combination

Pharmaceuticals	No	Molecular Name	MW	OB(%)	DL	Mol ID	PubChem CID
Astragalus	A1	(24S)-24-Propylcholesta-5-ene-3beta-ol	428.7	36.23	0.78	MOL000033	15976101
	A-L-1	Quercetin	302.23	46.43	0.28	MOL000098	5280343
	A3	Mairin	456.7	55.38	0.78	MOL000211	64971
	A4	Jaranol	314.29	50.83	0.29	MOL000239	5318869
	A5	Hederagenin	472.7	36.91	0.75	MOL000296	73299
	A6	Isorhamnetin	316.26	49.60	0.31	MOL000354	5281654
	A7	3,9-di-O-methylnissolin	314.3	53.74	0.48	MOL000371	15689655
	A8	7-O-Methylisomucronulatol	316.3	74.69	0.30	MOL000378	15689652
	A9	Methylnissolin	300.3	64.26	0.42	MOL000380	14077830
	A10	Bifendate	418.3	31.10	0.67	MOL000387	108213
	A11	Formononetin	268.26	69.68	0.21	MOL000392	5280378
	A12	Calycosin	284.26	47.75	0.24	MOL000417	5280448
	A-L-2	Kaempferol	286.24	41.89	0.24	MOL000422	5280863
	A14	FA	441.4	68.96	0.71	MOL000433	241106144
	A15	(3R)-3-(2-hydroxy-3,4-dimethoxyphenyl)chroman-7-ol	302.32	67.67	0.26	MOL000438	10380176
	A16	Isomucronulatol-7,2'-di-O-glucosiole	464.5	49.28	0.62	MOL000439	125142
	A17	1,7-Dihydroxy-3,9-dimethoxy pterocarpene	314.29	39.05	0.48	MOL000442	5316760
Ligustrum	L1	Luteolin	286.25	36.16	0.25	MOL000006	5280445
	A-L-1	Quercetin	302.25	46.43	0.28	MOL000098	5280343
	L3	Beta-sitosterol	414.79	36.91	0.75	MOL000358	222284
	A-L-2	Kaempferol	286.25	41.88	0.24	MOL000422	5280863
	L5	Taxifolin	304.27	57.84	0.27	MOL004576	439533
	L6	Lucidumoside D	568.63	48.87	0.71	MOL005146	10531060
	L7	Lucidumoside D_qt	406.47	54.41	0.47	MOL005147	-

MW: molecular weight; OB: oral bioavailability;DL: drug likeness;

Pharmaceuticals	No	Molecular Name	MW	OB(%)	DL	Mol ID	PubChem CID
	L8	(20S)-24-ene-3β,20-diol-3-acetate	486.86	40.23	0.82	MOL005169	-
	L9	Eriodictyol	288.27	71.79	0.24	MOL005190	440735
	L10	Syringaresinol diglucoside_qt	450.48	83.13	0.80	MOL005195	-
	L11	Lucidusculine	401.6	30.11	0.75	MOL005209	101286217
	L12	Olitoriside	696.87	65.45	0.23	MOL005211	94348
	L13	Olitoriside_qt	404.55	103.23	0.78	MOL005212	-

MW: molecular weight; OB: oral bioavailability;DL: drug likeness;

3.2 Acquisition of NSCLC-related targets and common targets of drugs and diseases

The 792 NSCLC disease-related target proteins were collected from Drugbank, Genecards and OMIM databases, and then merged and de-duplicated. The online software Venny 2.1.0 was used to intersect the 792 NSCLC disease targets with the 570 component targets standardized in "2.1" to obtain 180 anti-NSCLC targets of "*Astragalus-Ligustrum*" drug pair (Fig. 2).

3.3 Active ingredient-target network construction

The topological analysis of the 180 active targets of the "*Astragalus-Ligustrum*" drug pair against NSCLC obtained in "2.2" was carried out by constructing a network with its active ingredients (Fig. 3), The top 10 active ingredients were A-L-1 Quercetin, A-L-2Kaempferol, A6 Isorhamnetin, A4 Jaranol, A9 Methylnissolin, A15 (3R)-3-(2-hydroxy-3,4-dimethoxyphenyl) chroman-7-ol, A7 3,9-di-O-methylnissolin, A8 7-O-Methylisomucronulatol, L1 Luteolin, L9 Eriodictyol. Among the above, A-L-1 Quercetin, A-L-2Kaempferol can be found in both Astragalus and Ligustrum, L1 Luteolin, L9 Eriodictyol can be found in Ligustrum. The rest are the active ingredients in Astragalus. These components may be the core active ingredients of the "Astragalus-Ligustrum" drug pair against NSCLC, thus forming a complex network of drug-component-target-disease interactions. Each active ingredient acts on multiple targets, and each target has multiple active ingredients acting on it, reflecting the multi-component and multi-target mechanism of action of the "*Astragalus-Ligustrum*" drug pair against NSCLC.

3.4 Protein interactions (PPI) network construction and key proteins screening

The 180 interacting targets were imported into the STRING platform to obtain protein interaction relationships and plot the PPI network (Fig. 4). The magnitude of the degree value in the figure reflects the size of the node, and the color gradient is related to the betweenness centrality. The thickness of the edge and the gradient of the color are adjusted by the Edge betweenness and Combined score, respectively. The bigger the circle and the darker the color, the more of the protein is associated with other proteins in the whole network, and the more important it is. The highest confidence level (> 0.900) was chosen, and the average node degree value of the network was 13.3. The top 11 (3 times the average node degree value) protein targets were obtained by CytoScape analysis, which were TP53 (Degree = 57), SRC (Degree = 56), STAT3 (Degree = 55), PIK3R1 (Degree = 50), AKT1 (Degree = 50), HSP90AA1 (Degree = 49), MAPK3

(Degree = 49), MAPK1 (Degree = 46), PIK3CA (Degree = 45), JUN (Degree = 39), RELA (Degree = 39). These protein targets are at the core of the potential key targets of “Astragalus-Ligustrum” drug pair for the treatment of NSCLC, and the network was analyzed, edited and visualized by Cytoscape.

3.5 GO functional analysis and KEGG pathway analysis

GO functional analysis and KEGG signaling pathway enrichment analysis were performed on 180 intersecting targets of "Astragalus-Ligustrum" drug pair for NSCLC treatment by Metascape database, in which, GO analysis identified 221 biological process (BP), 77 cellular component (CC) and 95 molecular function (MF). Among the results of GO analysis, BP changes were mainly in the regulation of protein and amino acid phosphorylation, autophosphorylation and cell surface receptor and transmembrane receptor-mediated signaling pathways, involving protein phosphorylation, enzyme-linked receptor protein signaling pathway, response to growth factor, cellular response to growth factor stimulus, transmembrane receptor protein tyrosine kinase signaling pathway, protein autophosphorylation, peptidyl-tyrosine modification, peptidyl-tyrosine phosphorylation, regulation of phosphatidylinositol 3-kinase signaling, peptidyl-tyrosine autophosphorylation and other biological processes in which Genes were enriched.

CC changes in membrane rafts and associated protein kinase complexes, as evidenced by the enrichment of genes in membrane microdomain, membrane raft, transferase complex, transferring phosphorus-containing groups, cell-substrate junction, focal adhesion, plasma membrane raft, caveola, protein kinase complex, serine/threonine protein kinase complex and cyclin-dependent protein kinase holoenzyme complex.

The changes in MF were focused on kinase activity and enzyme binding, mainly related to related enzyme functions like kinase binding, protein kinase binding, protein serine/threonine kinase activity, protein serine kinase activity, kinase activity, phosphotransferase activity, alcohol group as acceptor, protein kinase activity, protein serine/threonine/tyrosine kinase activity, protein tyrosine kinase activity and transmembrane receptor protein tyrosine kinase activity. The top 10 positions were selected based on the results of "Gene Counts" for visualization (Fig. 5a)

A total of 221 results were obtained from KEGG enrichment analysis, and the top 10 signaling pathways were selected for visualization based on "P-value" (Fig. 5b). The results mainly involved the PI3K-Akt signaling pathway, FoxO signaling pathway, PD-L1 expression and PD-1 checkpoint pathway in cancer, C-type lectin receptor signaling pathway, TNF signaling pathway, IL-17 signaling pathway, T cell receptor signaling pathway, Toll-like receptor signaling pathway, NOD-like receptor signaling pathway and NF-kappa B signaling pathway. This result suggests that the "*Astragalus-Ligustrum*" drug pair may play a role in the treatment of NSCLC through multiple signaling pathways.

3.6 Molecular docking

The potential core active ingredients of *"Astragalus-Ligustrum*" drug pair (Quercetin, Kaempferol Isorhamnetin, Jaranol, Methylnissolin, (3R)-3-(2-hydroxy-3,4-dimethoxyphenyl) chroman-7-ol, 3,9-di-O-methylnissolin, 7-OMethylisomucronulatol, Luteolin,Eriodictyol)) were predicted to bind with the potential key targets TP53, SRC, STAT3, PIK3R1, AKT1 and the pathway-related core targets PD-1 and PD-L1 by the above network pharmacology method. Generally, the lower the binding energy of the ligand to the receptor, the more stable the binding conformation and the better the binding ability. Binding energies less than − 4.25 kcal- mol-1 suggest some ligand-receptor binding activity, less than − 5.0 kcal- mol-1 good binding activity, and less than − 7.0 kcal- mol-1 strong binding activity [31]. The above 10 potential core active ingredients were docked with 5 potential core target proteins, and the results showed that all the active ingredients had strong binding activity with TP53, SRC, STAT3, PIK3R1, AKT1, PD-1, PDL1, and especially with AKT1 and PD-L1, except for huperzine, which had low binding activity with PD-1 receptor protein, as shown in Fig. 6a. The docking results with strong binding activity (< -9.60 kcal- mol-1) in Astragalus chasteensis(Fig. 6b) were

visualized by PyMOL software to demonstrate the molecular docking technique to predict the binding ability of the core components of "*Astragalus-Ligustrum*" to the target.

3.7 MD simulation analysis

The RMSD of all the atoms in the complex was varied with time (Fig. 7a), and the RMSD of the complex only increased slightly at the beginning of the whole simulation process and stabilized around 5 ns; then there was a small fluctuation between 10–15 ns, and it was speculated that the conformation of the small molecule and the protein had changed due to the interaction, which made the binding between them more stable. The mean value of RMSD for the whole process was 0.420 ± 0.127 nm, indicating that the kinetic simulation was stable and reliable based on the force field parameters, which could be used for further analysis. Figure 7b gives the Rg of the whole complex system with the simulation time, and it can be found that the Rg of the whole system is relatively stable during the simulation, and there is no obvious large fluctuation, and the average value of Rg is 2.849 ± 0.033 nm during the whole process. The SASA of the whole system was expanded due to the interaction between the external amino acid residues and the solvent at the beginning of the simulation (Fig. 7c). The corresponding SASA became larger; then it started to decrease and stabilize around 5 ns, indicating that the protein complex was basically stabilized in the solvent system at this time. The overall SASA of the stabilized structure was smaller than the initial structure, and the structure of the complex was more compact. The binding free energy between protein and small molecules (Table 2) was calculated with the help of MM/PBSA method in the more stable 15–20 ns interval of RMSD. The total binding free energy between small molecules and proteins is -142.486 kJ/mol, in which the electrostatic interaction of the system including the electrostatic interaction under vacuum conditions and the polar solvation energy (ΔGele + ΔGPB) is 80.046 kJ/mol; the non-polar interaction can be used as the hydrophobic interaction energy, including the van der Waals force interaction and the non-polar solvation free energy (ΔGvdw + ΔGPB). energy (ΔGvdw + ΔGnp) with −222.532 kJ/mol for the non-polar interaction.

Table 2
Different Free Energy of Binding of Small Molecules to Protein

Item	Energy(kJ/mol)	Delta
ΔGvdw(kJ/mol)	-207.915	22.359
ΔGele(kJ/mol)	-22.111	6.157
ΔGPB(kJ/mol)	102.157	17.110
ΔGnp(kJ/mol)	-14.617	1.215
ΔGbind(kJ/mol)	-142.486	15.209
ΔG vdw: van der Waals; ΔG ele: electrostatic energy; ΔGPB: gas phase basicity ; ΔGnp: non-polar solvation free energies; ΔGbind: The binding free energies		

Finally, the complex conformation after MD simulation was extracted and the interaction pattern between proteins was analyzed in this paper (Fig. 8). The protein and small molecule can bind tightly to the target protein in the active pocket through van der Waals, hydrophobic bonds and Pi bonds.

3.8 Survival curve analysis

The core genes of TP53, SRC, STAT3, PIK3R1, AKT1, PD-1, and PD-L1 screened by Cytoscape software were introduced into the Kaplan-Meier Plotter (Fig. 9). PDCD1 and PD-L1 (CD274) genes were statistically significant (P <

0.05) in relation to the overall survival rate. The overall survival rate of patients with low expression of TP53, SRC, AKT1, PD-1 (PDCD1), and PD-L1 (CD274) was better than that of the high expression group, while the overall survival rate of patients with high expression of PIK3R1 was better than that of the low expression group. To further characterize the gene expression levels in lung cancer versus normal subjects, the GEPIA2 website was used to analyze these five genes that may be associated with prognosis. TP53 had significant expression levels in lung squamous carcinoma specimens compared with normal specimens, and PIK3R1 and PD-L1 had significant differences in expression in both lung glandular and squamous carcinoma specimens (Fig. 10).

3.9 Immunohistochemical analysis

To further understand the differential expression of the key targets TP53, SRC, STAT3, PIK3R1, AKT1, PD-1, and PDL1 in lung cancer, validation of protein expression levels was tested. A search of the HPA database revealed that the expression of the proteins encoded by these key target genes were significantly different in normal lung tissues and lung tissues of lung cancer patients, as shown in Fig. 11. Among them, except for TP53, SRC, PD-1 and PD-L1, the other three genes were expressed in normal lung tissues to different degrees. Compared with normal lung tissues, PIK3R1 was lowly expressed in lung cancer tissues, while TP53, SRC, STAT3, AKT1, PD-1 and PD-L1 were expressed at elevated levels. These results further suggest that the abnormal expression of these targets at the protein level may have a relationship with the development of lung cancer.

4 Discussion

In this study, 28 active ingredients and 180 active ingredient targets were screened from the "*Astragalus-Ligustrum*" drug pair. By analyzing the "drug-active-component-target" network, 10 components, including quercetin, kaempferol, isorhamnetin, jaranol, methylnissolin, luteolin and eriodictyol, were identified as the main active components of "*Astragalus-Ligustrum*" drug pair in the treatment of NSCLC. The results suggest that the active ingredients were mainly flavonoids. Flavonoids are naturally occurring secondary metabolites, and more than 10,000 compounds have been reported [32], which are safe and easy to obtain and have a wide range of pharmacological activities. Numerous studies have shown that flavonoids have significant preventive and curative effects on many common cancers such as lung, breast, and colon cancers, and are considered as potential candidates for new anti-cancer therapies [33]. Quercetin and kaempferol are the common active ingredients of Astragalus and Ligustrum. Quercetin is a flavonol compound and an active ingredient in many herbal medicines with a wide range of anti-lung cancer mechanisms [34–35]. Kaempferol has been shown to have various biological activities such as antioxidant, anticancer, anti-inflammatory, atherosclerosis prevention, and protection of damaged cells [36–38]. In one study, kaempferol was found to target and destroy the nuclei of A549 lung cancer cells when combined with gold nanoclusters [39]. Isorhamnetin, hualanganin, astragalus rosmarinicus chroman-7-ol, (3R)-3-(2-hydroxy-3,4-dimethoxyphenyl) chroman-7-ol, 3,9-di-O-methylnisonic pea rosmarinicol, and 7-O-methyl-isomicroconvex sabinol are the active components from Astragalus. It has been shown that isorhamnetin can inhibit the proliferation and induce apoptosis of NSCLC cells, and its mechanism of action is related to the autophagic process[40]. Few studies have been reported on the rest of the active ingredients related to lung cancer. In addition, lignocaine and sageol are the active components from Ligustrum. Lignans significantly downregulated the expression levels of AIM2 mRNA and protein in NSCLC cells, thereby inhibiting the activation of AIM2 inflammatory vesicles, inducing G2/M phase arrest in cancer cells, and suppressing the EMT process to exert anti-tumor effects[41]. Sanguinarol exerted good antitumor effects on A549 human lung cancer cells by inducing mitochondria-mediated apoptosis, G2/M cell cycle arrest and inhibition of m-TOR/PI3K/Akt signaling pathway[42].

Among the top 10 active ingredients ranked by degree value, 8 active ingredients attributed to Astragalus and 4 active ingredients attributed to Ligustrum, indicating that "*Astragalus-Ligustrum*" drug pair plays a major role in the treatment of NSCLC. In the PPI network, TP53, SRC, STAT3, PIK3R1 and AKT1 were identified as the core targets in the network, which are the core targets of the "*Astragalus-Ligustrum*" drug pair in the treatment of NSCLC. TP53 is one of the first oncogenes identified, and mutations of TP53 are found in more than 50% of human tumors, mainly missense mutations[43, 44]. It has been reported that TP53-Mut is more common in squamous lung cancer than lung adenocarcinoma, with a mutation rate of 65%, and is highly correlated with smoking[45, 46]. TP53 mutations significantly increased immune checkpoint expression, activated effector T cells and increased interferon γ levels, and it is worth mentioning that the TP53/KRAS co-mutant subgroup showed increased PD-L1 expression and the highest PD-L1+/CD8A + ratio[47]. SRC is a member of the SRC tyrosine kinase family, and aberrant Src activation is associated with the development of several human tumors, including lung cancer, especially in adenocarcinoma, where SRC kinase activity shows high levels and the degree of kinase activity increases with tumor enlargement [48]. The association between SRC family kinase (SFK) member YES1 protein expression and The SFK inhibitor dasatinib acts synergistically with anti-PD-1 to inhibit tumor growth in experimental models of NSCLC[49]. STAT3, an important member of the signal transduction and transcriptional activator family, is a key signaling pathway molecule linking inflammation and tumor, and STAT3-targeted therapies are now expected to be a promising clinical strategy [50]. The AKT-STAT3 pathway is a downstream target of the EGFR signaling pathway, and Abdelhamed S et al found that inhibition of AKT and STAT3 activity could downregulate PD-L1 expression in gefitinib-resistant NSCLC, suggesting that STAT3 could be a potential therapeutic target for reversing acquired drug resistance in NSCLC[51]. PIK3R1, the p85 regulatory subunit of phosphatidylinositol 3 kinase, is considered as a tumor suppressor and is under-expressed in most tumors[52]. It is increasingly reported [53]that when PIK3R1 expression reduced in cancers such as lung and breast cancer, phosphorylation of PI3K and AKT enhanced, leading to increased classical AKT signaling in these tumorigenic phenotypes. AKT1 is one of the important isoforms of serine/threonine protein kinase, and studies suggest that its expression is upregulated as an oncogene in NSCLC, which is closely related to tumor progression and poor prognosis. It has been found [54]that the PI3K/AKT signaling pathway may affect the activity of immune cells in the tumor immune microenvironment and negatively regulate the expression of PD-L1 in NSCLC cells, but further studies are needed. In conclusion, TP53, SRC, STAT3, PIK3R1, AKT1 and other genes have been shown to be closely related to the development of NSCLC, and it is assumed that the "*Astragalus-Ligustrum*" drug pair mainly exerts regulatory effects through these targets to treat NSCLC. The molecular docking results showed that quercetin, kaempferol, isorhamnetin, and isorhamnetin were all used in the treatment of NSCLC. The molecular docking results showed that the core active ingredients such as quercetin, kaempferol, isorhamnetin, astragaloside, 7-O-methyl-isoconvex sarcosol, lignan, sage phenol and TP53, SRC, STAT3, PIK3R1, AKT1, PD-1 and PD-L1 had strong binding activities, which suggested that the results of this study were reliable.

The potential targets of "*Astragalus-Ligustrum*" drug pair for the treatment of NSCLC mainly involved protein phosphorylation, enzyme-linked receptor protein signaling pathway, cellular response to growth factor stimulation, transmembrane receptor protein tyrosine kinase signaling pathway and other biological processes through GO bio-functional analysis. The enriched cellular fractions are mainly localized in the membrane raft and associated protein kinase complex fractions and are predominantly involved in biological functions such as kinase binding and activity. These biological processes are reflected in the targets and related pathways involved in drug resistance against NSCLC. Among them, protein kinases are a class of phosphotransferases that mainly contribute to protein phosphorylation, which is involved in most of the important life processes in cells. It has been demonstrated that flavonoids have inhibitory effects on mitogen-activated protein kinases, cytokinin-dependent protein kinases, PI3K and Akt/protein kinase B, thereby interfering with cell signaling, inducing apoptosis and inhibiting cancer cell proliferation, promoting oncogene expression and suppressing oncogene expression[55, 56]. KEGG enrichment analysis revealed

that KEGG enrichment analysis showed that "*Astragalus-Ligustrum*" drug pair treatment of NSCLC involves several classical signaling pathways clearly associated with lung cancer, including PI3K-Akt, FoxO, PD-1/PD-L1, C-type lectin receptor, TNF, IL-17, T-cell receptor, Toll-like receptor, NOD-like receptor, NF-κB, etc. The PI3K-Akt pathway is currently one of the most important regulatory pathways in NSCLC and plays an important role in promoting NSCLC proliferation and metastasis, inducing epithelial-mesenchymal transition (EMT), and influencing acquired drug resistance in lung cancer [57–59]. There are many types of pathways in the entire KEGG database that are directly or indirectly related to PI3K-Akt. Upon activation of PI3K-Akt signaling, it is transmitted to downstream pathways, leading to the activation of a series of pathways, which include mTOR, VEGF, MAPK, FoxO, NF-κB, etc. PI3K-Akt can also be activated by multiple upstream pathways, which PI3K-Akt can also be activated by multiple upstream pathways, and these upstream signals can originate from PD-1/PD-L1, Toll-like receptors, B-cell receptors, JAK/STAT and other signaling pathways, so PI3K-Akt signaling pathway can be downstream of multiple signaling processes, or it is a very critical step of many signaling pathways. Another report showed that the PI3K-Akt pathway mediates immune escape of tumor cells by affecting the activity of immune cells in tumor microenvironment and the expression of PD-L1, which is involved in the formation of an immunosuppressive microenvironment [60]. The pathways mainly attributed to the immune system in the present findings are PD-1/PD-L1, NOD-like receptors, C-type lectin receptors, Toll-like receptors, T-cell receptors, and IL-17, and there are numerous studies showing that these pathways are closely related to the development of NSCLC [61]. Besides, TNF is a classical inflammatory, tumor and immune-related signaling pathway, and TNF-α may act as a tumor promoter gene, and in NSCLC TNF-α may regulate the cell cycle by activating the NF-κB signaling pathway, which in turn affects cell proliferation and apoptosis [62]. It is worth noting that these signaling pathways are mostly related to immune response and inflammation, suggesting that the treatment of NSCLC disease with "*Astragalus-Ligustrum*" drug pair may involve multiple pathways and targets, but focus on immune and inflammatory aspects. In combination with core target analysis, TP53, SRC, STAT3, PIK3R1 and AKT1 also play important roles in the PD-1/PD-L1 signaling pathway. Cancer immunotherapy is an increasingly successful strategy for the treatment of patients with advanced or conventional treatment-resistant cancers, and T cells are key mediators of tumor destruction, where they are critical for the specificity of tumor-expressed antigens. Based on this, further study will subsequently focus on the mechanisms associated with the PD-1/PD-L1, the negative regulatory signaling pathway for T cell activation.

In conclusion, 28 active ingredients and 180 active ingredient targets were screened from the "*Astragalus-Ligustrum*" drug pair. 10 components, including quercetin and kaempferol were identified as the main active components in the treatment of NSCLC. It affects protein phosphorylation, cellular response to growth factor stimulation and other biological processes, regulates PI3K-Akt, PD-1/PD-L1 and other lung cancer-related pathways, and then intervenes in the process of NSCLC. Further molecular kinetic results showed that the complex could bind to the target protein in the active pocket through van der Waals, hydrophobic and Pi bonds between the protein and small molecules. The binding activity between PD-L1 and the main active ingredient may be one of the important mechanisms of the anti-NSCLC action of "Astragalus-Ligustrum" drug pair. The predicted results are close to the modern pharmacological research results, which also support the feasibility of this study, and fit the holistic and systematic characteristics of Chinese medicine. Given that this is only an exploration at the level of molecular mechanism, basic experiments still need to be used subsequently to further validate its accuracy.

Abbreviations

NSCLC: Non-Small Cell Lung Cancer

SCLC: Small Cell Lung Cancer

TCMSP: Traditional Chinese Medicine Systems Pharmacology Database and Analysis Platform

ADME: Absorption Distribution Metabolism and Excretion

OB: Oral Bioavailability

DL: Drug Likeness

OMIM: Online Mendelian Inheritance in Man

PPI: Protein-Protein Interaction

GO: Gene Ontology

KEGG: Kyoto Encyclopedia of Genes and Genomes

BP: Biological Process

CC: Cellular Component

MF: Molecular Function

PDB: Protein Data Bank

MD: Molecular dynamics

LINCS: Linear Constraint Solver

PME : Particle-mesh Ewald

HPA: Human Protein Atlas

MW: Molecular Weight

RMSD: Root Mean Square Deviation

RMSF: Root Mean Square Fluctuation

Rg: Radius of Gyration

LUAD: Lung Adenocarcinoma

LUSC: Lung Squamous Cell Carcinoma

EMT: Epithelial-mesenchymal Transition

Declarations

Data availability

The datasets generated during and/or analysed during the current study are available from the corresponding author on reasonable request.

Acknowledgements

We as authors appreciate anonymous reviewers for their insightful comments to improve this work.

Funding

This work was supported by Taizhou Traditional Chinese Medicine Technology Development Project (Grant numbers [TZ202205]. Author Zhengting Deng has received this research support. This work was also supported by National Natural Science Foundation of China Youth Fund (Grant numbers [82104977]. Author Tong Zhao has received this research support.

Author information

Authors and Affiliations

Authors and their affiliations.

Taizhou Hospital Affiliated to Nanjing University of Chinese Medicine, Taizhou 225300, Jiangsu Province, China

Zhengting Deng, Hu Tian, Yuanhua Ding, Qiming Jin

School of Chinese Medicine, School of Integrated Chinese and Western Medicine, Nanjing University of Chinese Medicine, Nanjing 210023, Jiangsu Province, China

Tong Zhao, Yichen Liu, Tao Liu

Shen Chun-ti Nation-Famous Experts Studio for Traditional Chinese Medicine Inheritance Changzhou TCM Hospital Affiliated to Nanjing University of Chinese Medicine, Changzhou, China

Tong Zhao

Contributions

All authors contributed to the study conception and design. Material preparation, data collection and analysis were performed by Zhengting Deng, Tong Zhao and Tao Liu. The first draft of the manuscript was written by Zhengting Deng and all authors commented on previous versions of the manuscript. All authors read and approved the final manuscript.

Corresponding author

Correspondence to Tao Liu

Declaration of competing interest

The authors declare that they have no known competing financial interests or personal relationships that could have appeared to influence the work reported in this paper.

References

1. Ettinger DS, Wood DE, Aisner DL, Akerley W, Bauman JR, Bharat A, et al. Non-small cell lung cancer, version 3.2022, nccn clinical practice guidelines in oncology. J Natl Compr Canc Netw 2022; 20(5):497-530.

2. Men Y, Wang L, Zhang Y, Gao S, Li J, Wu N, et al. Trends of postoperative radiotherapy for completely resected non-small cell lung cancer in china: a hospital-based multicenter 10-year (2005-2014) retrospective clinical epidemiological study. Front Oncol 2019; 9:786.
3. Singal G, Miller PG, Agarwala V, Li G, Kaushik G, Backenroth D, et al. Association of patient characteristics and tumor genomics with clinical outcomes among patients with non-small cell lung cancer using a clinicogenomic database. Jama 2019; 321(14):1391-9.
4. Ettinger DS, Wood DE, Aisner DL, Akerley W, Bauman JR, Bharat A, et al. Non-small cell lung cancer, version 3.2022, nccn clinical practice guidelines in oncology. J Natl Compr Canc Netw 2022; 20(5):497-530.
5. Xu B, Ge Y, Wyg H, Zhang X, Wu J, Li J. Efficacy and safety of east asian herbal medicine for brain metastases in non-small cell lung cancer: a systematic review and meta-analysis protocol to identify specific herbs. Integr Cancer Ther 2023; 22:1553465137.
6. Doroshow DB, Bhalla S, Beasley MB, Sholl LM, Kerr KM, Gnjatic S, et al. Pd-l1 as a biomarker of response to immune-checkpoint inhibitors. Nat Rev Clin Oncol 2021; 18(6):345-62.
7. Li JS, Liu XF, Dong HR, Zheng WC, Feng SX, Tian YG, et al. Effective-constituent compatibility-based analysis of bufei yishen formula, a traditional herbal compound as an effective treatment for chronic obstructive pulmonary disease. J Integr Med 2020; 18(4):351-62.
8. Bukhari S, Hussain F, Thu HE, Hussain Z. Synergistic effects of combined therapy of curcumin and fructus ligustri lucidi for treatment of osteoporosis: cellular and molecular evidence of enhanced bone formation. J Integr Med 2019; 17(1):38-45.
9. Zhou Y, Wu C, Qian X, Zhou J, Li C, Jiao Y, et al. Multitarget and multipathway regulation of zhenqi fuzheng granule against non-small cell lung cancer based on network pharmacology and molecular docking. Evid Based Complement Alternat Med 2022; 2022:5967078.
10. Ru J, Li P, Wang J, Zhou W, Li B, Huang C, et al. Tcmsp: a database of systems pharmacology for drug discovery from herbal medicines. J Cheminform 2014; 6:13.
11. Kim S, Chen J, Cheng T, Gindulyte A, He J, He S, et al. Pubchem in 2021: new data content and improved web interfaces. Nucleic Acids Res 2021; 49(D1):D1388-95.
12. Joshi AA, Khairnar SV, Chaudhari HK. In silico adme/pharmacokinetic and target prediction studies of ethambutol as drug molecule. Infect Disord Drug Targets 2022; 22(4):e1417407573.
13. . Uniprot: the universal protein knowledgebase in 2021. Nucleic Acids Res 2021; 49(D1):D480-9.
14. Luo Y, Fu Y, Tan T, Hu J, Li F, Liao Z, et al. Screening of lncrna-mirna-mrna coexpression regulatory networks involved in acute traumatic coagulation dysfunction based on ctd, genecards, and pharmgkb databases. Oxid Med Cell Longev 2022; 2022:7280312.
15. M R, M A, H B, M O. Global single clustering of phenotype-associated human aging genes in the co-expression and physical interaction networks: an omim-based investigative review. Arch Gerontol Geriatr 2021; 96:104461.
16. Wishart DS, Feunang YD, Guo AC, Lo EJ, Marcu A, Grant JR, et al. Drugbank 5.0: a major update to the drugbank database for 2018. Nucleic Acids Res 2018; 46(D1):D1074-82.
17. Szklarczyk D, Gable AL, Nastou KC, Lyon D, Kirsch R, Pyysalo S, et al. The string database in 2021: customizable protein-protein networks, and functional characterization of user-uploaded gene/measurement sets. Nucleic Acids Res 2021; 49(D1):D605-12.
18. Zhou Y, Zhou B, Pache L, Chang M, Khodabakhshi AH, Tanaseichuk O, et al. Metascape provides a biologist-oriented resource for the analysis of systems-level datasets. Nat Commun 2019; 10(1):1523.

19. . Protein data bank: the single global archive for 3d macromolecular structure data. Nucleic Acids Res 2019; 47(D1):D520-8.
20. Zhou Y, Wu C, Qian X, Zhou J, Li C, Jiao Y, et al. Multitarget and multipathway regulation of zhenqi fuzheng granule against non-small cell lung cancer based on network pharmacology and molecular docking. Evid Based Complement Alternat Med 2022; 2022:5967078.
21. Kutzner C, Pall S, Fechner M, Esztermann A, de Groot BL, Grubmuller H. More bang for your buck: improved use of gpu nodes for gromacs 2018. J Comput Chem 2019; 40(27):2418-31.
22. Sheng YJ, Yin YW, Ma YQ, Ding HM. Improving the performance of mm/pbsa in protein-protein interactions via the screening electrostatic energy. J Chem Inf Model 2021; 61(5):2454-62.
23. Shaik MS, Liem SY, Popelier PL. Properties of liquid water from a systematic refinement of a high-rank multipolar electrostatic potential. J Chem Phys 2010; 132(17):174504.
24. Xie Z, Kropiwnicki E, Wojciechowicz ML, Jagodnik KM, Shu I, Bailey A, et al. Getting started with lincs datasets and tools. Curr Protoc 2022; 2(7):e487.
25. Simmonett AC, Brooks BR. Analytical hessians for ewald and particle mesh ewald electrostatics. J Chem Phys 2021; 154(10):104101.
26. Karwasra R, Fatihi S, Raza K, Singh S, Khanna K, Sharma S, et al. Filgrastim loading in plga and sln nanoparticulate system: a bioinformatics approach. Drug Dev Ind Pharm 2020; 46(8):1354-61.
27. Martonak R, Laio A, Parrinello M. Predicting crystal structures: the parrinello-rahman method revisited. Phys Rev Lett 2003; 90(7):75503.
28. Qi Q, Huang W, Zhang H, Zhang B, Sun X, Ma J, et al. Bioinformatic analysis of plod family member expression and prognostic value in non-small cell lung cancer. Transl Cancer Res 2021; 10(6):2707-24.
29. Tang Z, Kang B, Li C, Chen T, Zhang Z. Gepia2: an enhanced web server for large-scale expression profiling and interactive analysis. Nucleic Acids Res 2019; 47(W1):W556-60.
30. Miura K, Ishida K, Fujibuchi W, Ito A, Niikura H, Ogawa H, et al. Differentiating rectal carcinoma by an immunohistological analysis of carcinomas of pelvic organs based on the ncbi literature survey and the human protein atlas database. Surg Today 2012; 42(6):515-25.
31. Zhang B, Wang M, Sun Y, Zhao P, Liu C, Qing K, et al. Glycine max nnl1 restricts symbiotic compatibility with widely distributed bradyrhizobia via root hair infection. Nat Plants 2021; 7(1):73-86.
32. Dixon RA, Pasinetti GM. Flavonoids and isoflavonoids: from plant biology to agriculture and neuroscience. Plant Physiol 2010; 154(2):453-7.
33. Tang SM, Deng XT, Zhou J, Li QP, Ge XX, Miao L. Pharmacological basis and new insights of quercetin action in respect to its anti-cancer effects. Biomed Pharmacother 2020; 121:109604.
34. Guo H, Ding H, Tang X, Liang M, Li S, Zhang J, et al. Quercetin induces pro-apoptotic autophagy via sirt1/ampk signaling pathway in human lung cancer cell lines a549 and h1299 in vitro. Thorac Cancer 2021; 12(9):1415-22.
35. Imran M, Salehi B, Sharifi-Rad J, Aslam GT, Saeed F, Imran A, et al. Kaempferol: a key emphasis to its anticancer potential. Molecules 2019; 24(12).
36. Feng Z, Wang C, Yue, Jin, Meng Q, Wu J, et al. Kaempferol-induced gper upregulation attenuates atherosclerosis via the pi3k/akt/nrf2 pathway. Pharm Biol 2021; 59(1):1106-16.
37. Binmowyna MN, Alfaris NA. Kaempferol suppresses acetaminophen-induced liver damage by upregulation/activation of sirt1. Pharm Biol 2021; 59(1):146-56.
38. Govindaraju S, Roshini A, Lee MH, Yun K. Kaempferol conjugated gold nanoclusters enabled efficient for anticancer therapeutics to a549 lung cancer cells. Int J Nanomedicine 2019; 14:5147-57.

39. Ruan Y, Hu K, Chen H. Autophagy inhibition enhances isorhamnetin-induced mitochondria-dependent apoptosis in non-small cell lung cancer cells. Mol Med Rep 2015; 12(4):5796-806.
40. Yu Q, Zhang M, Ying Q, Xie X, Yue S, Tong B, et al. Decrease of aim2 mediated by luteolin contributes to non-small cell lung cancer treatment. Cell Death Dis 2019; 10(3):218.
41. Zhang Y, Zhang R, Ni H. Eriodictyol exerts potent anticancer activity against a549 human lung cancer cell line by inducing mitochondrial-mediated apoptosis, g2/m cell cycle arrest and inhibition of m-tor/pi3k/akt signalling pathway. Arch Med Sci 2020; 16(2):446-52.
42. Kastenhuber ER, Lowe SW. Putting p53 in context. Cell 2017; 170(6):1062-78.
43. Lu P, White-Gilbertson S, Beeson G, Beeson C, Ogretmen B, Norris J, et al. Ceramide synthase 6 maximizes p53 function to prevent progeny formation from polyploid giant cancer cells. Cancers (Basel) 2021; 13(9).
44. Halvorsen AR, Silwal-Pandit L, Meza-Zepeda LA, Vodak D, Vu P, Sagerup C, et al. Tp53 mutation spectrum in smokers and never smoking lung cancer patients. Front Genet 2016; 7:85.
45. Ozaki Y, Muto S, Takagi H, Watanabe M, Inoue T, Fukuhara M, et al. Tumor mutation burden and immunological, genomic, and clinicopathological factors as biomarkers for checkpoint inhibitor treatment of patients with non-small-cell lung cancer. Cancer Immunol Immunother 2020; 69(1):127-34.
46. Dong ZY, Zhong WZ, Zhang XC, Su J, Xie Z, Liu SY, et al. Potential predictive value of tp53 and kras mutation status for response to pd-1 blockade immunotherapy in lung adenocarcinoma. Clin Cancer Res 2017; 23(12):3012-24.
47. Masaki T, Igarashi K, Tokuda M, Yukimasa S, Han F, Jin YJ, et al. Pp60c-src activation in lung adenocarcinoma. Eur J Cancer 2003; 39(10):1447-55.
48. Redin E, Garmendia I, Lozano T, Serrano D, Senent Y, Redrado M, et al. Src family kinase (sfk) inhibitor dasatinib improves the antitumor activity of anti-pd-1 in nsclc models by inhibiting treg cell conversion and proliferation. J Immunother Cancer 2021; 9(3).
49. Liu Z, Ma L, Sun Y, Yu W, Wang X. Targeting stat3 signaling overcomes gefitinib resistance in non-small cell lung cancer. Cell Death Dis 2021; 12(6):561.
50. Abdelhamed S, Ogura K, Yokoyama S, Saiki I, Hayakawa Y. Akt-stat3 pathway as a downstream target of egfr signaling to regulate pd-l1 expression on nsclc cells. J Cancer 2016; 7(12):1579-86.
51. Liu Y, Wang D, Li Z, Li X, Jin M, Jia N, et al. Pan-cancer analysis on the role of pik3r1 and pik3r2 in human tumors. Sci Rep 2022; 12(1):5924.
52. Liu Y, Wang D, Li Z, Li X, Jin M, Jia N, et al. Pan-cancer analysis on the role of pik3r1 and pik3r2 in human tumors. Sci Rep 2022; 12(1):5924.
53. Gao Y, Yang J, Cai Y, Fu S, Zhang N, Fu X, et al. Ifn-gamma-mediated inhibition of lung cancer correlates with pd-l1 expression and is regulated by pi3k-akt signaling. Int J Cancer 2018; 143(4):931-43.
54. Cayetano-Salazar L, Nava-Tapia DA, Astudillo-Justo KD, Arizmendi-Izazaga A, Sotelo-Leyva C, Herrera-Martinez M, et al. Flavonoids as regulators of timps expression in cancer: consequences, opportunities, and challenges. Life Sci 2022; 308:120932.
55. Chae HS, Xu R, Won JY, Chin YW, Yim H. Molecular targets of genistein and its related flavonoids to exert anticancer effects. Int J Mol Sci 2019; 20(10).
56. Jiang M, Zhou LY, Xu N, An Q. Hydroxysafflor yellow a inhibited lipopolysaccharide-induced non-small cell lung cancer cell proliferation, migration, and invasion by suppressing the pi3k/akt/mtor and erk/mapk signaling pathways. Thorac Cancer 2019; 10(6):1319-33.

57. Jia Z, Zhang Y, Xu Q, Guo W, Guo A. Mir-126 suppresses epithelial-to-mesenchymal transition and metastasis by targeting pi3k/akt/snail signaling of lung cancer cells. Oncol Lett 2018; 15(5):7369-75.
58. Li Y, Wu Y, Xia Q, Zhao Y, Zhao R, Deng S. Platycodon grandiflorus enhances the effect of ddp against lung cancer by down regulating pi3k/akt signaling pathway. Biomed Pharmacother 2019; 120:109496.
59. Wu J, Zhao X, Sun Q, Jiang Y, Zhang W, Luo J, et al. Synergic effect of pd-1 blockade and endostar on the pi3k/akt/mtor-mediated autophagy and angiogenesis in lewis lung carcinoma mouse model. Biomed Pharmacother 2020; 125:109746.
60. Liotti F, Marotta M, Sorriento D, Pone E, Morra F, Melillo RM, et al. Toll-like receptor 7 mediates inflammation resolution and inhibition of angiogenesis in non-small cell lung cancer. Cancers (Basel) 2021; 13(4).
61. Zhao C, Li Y, Zhang W, Zhao D, Ma L, Ma P, et al. Il-17 induces nsclc a549 cell proliferation via the upregulation of hmga1, resulting in an increased cyclin d1 expression. Int J Oncol 2018; 52(5):1579-92.

Figures

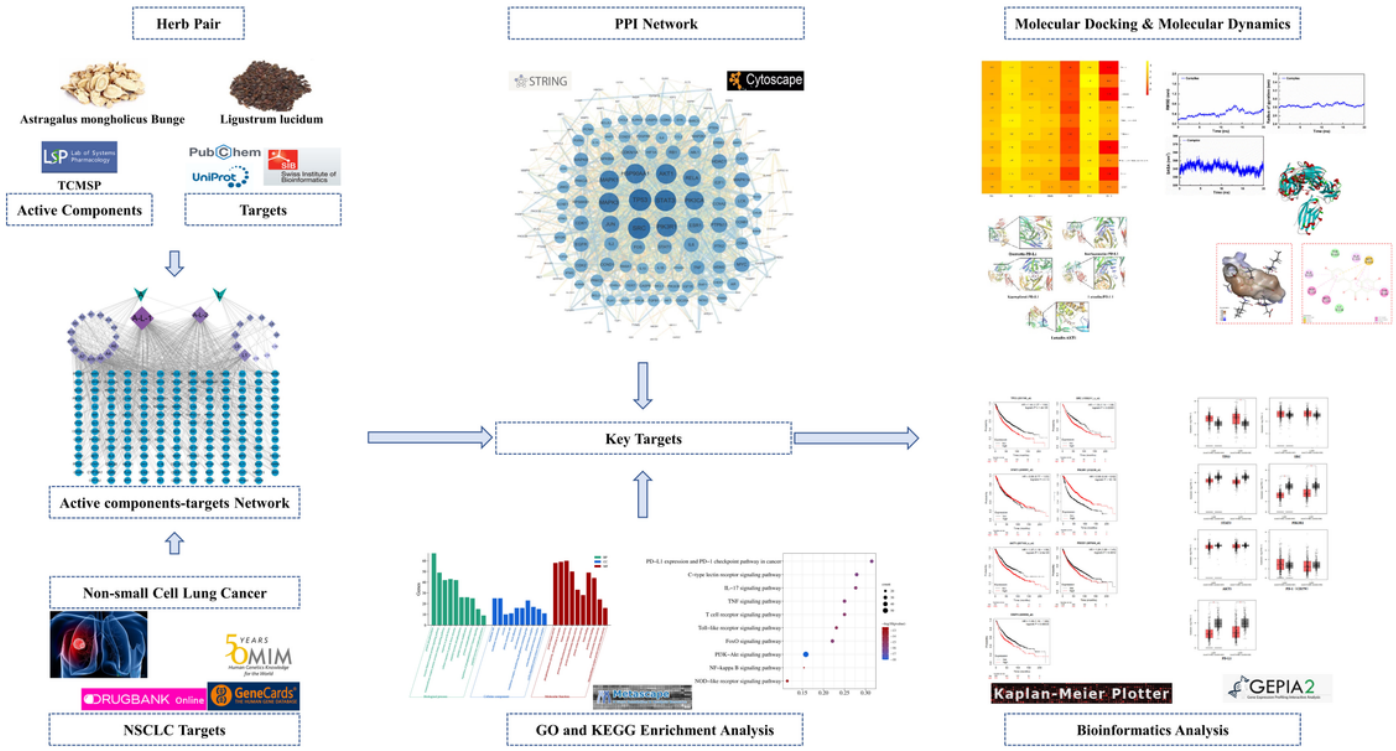


Figure 1

The protocol of study procedures

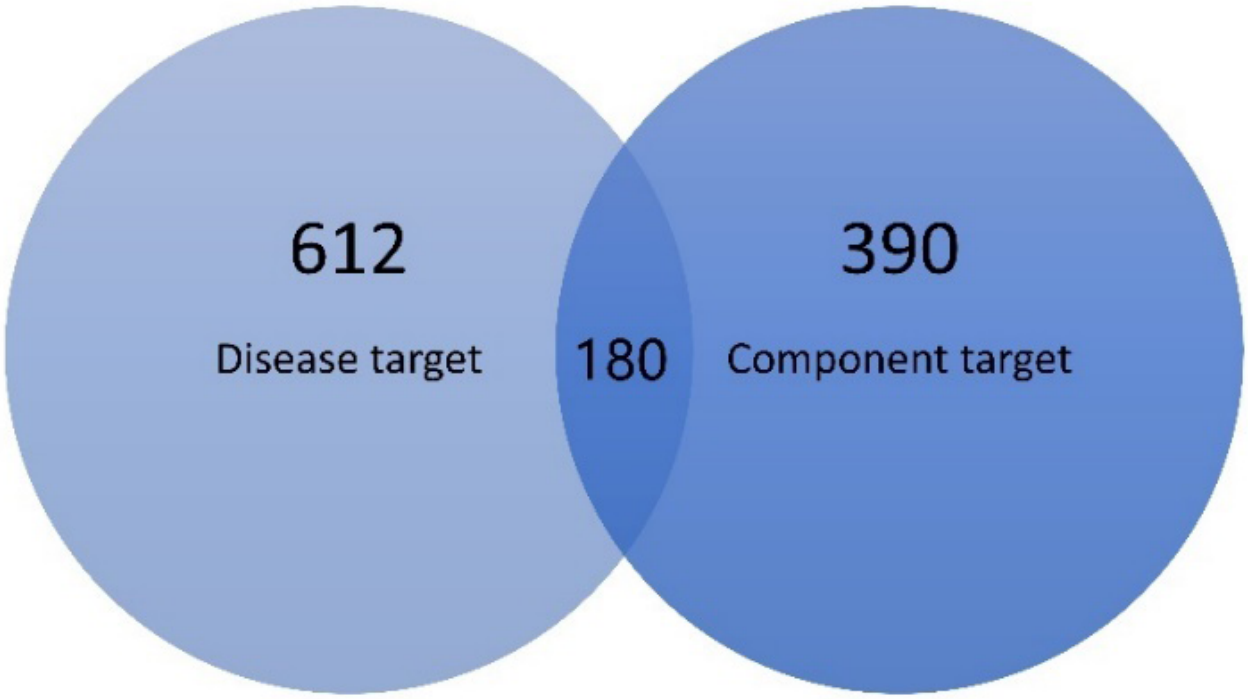


Figure 2

Venn diagram of "*Astragalus–Ligustrum*" drug pair in treatment of NSCLC

180 means the number of anti-NSCLC targets of "Astragalus-Ligustrum" drug pair

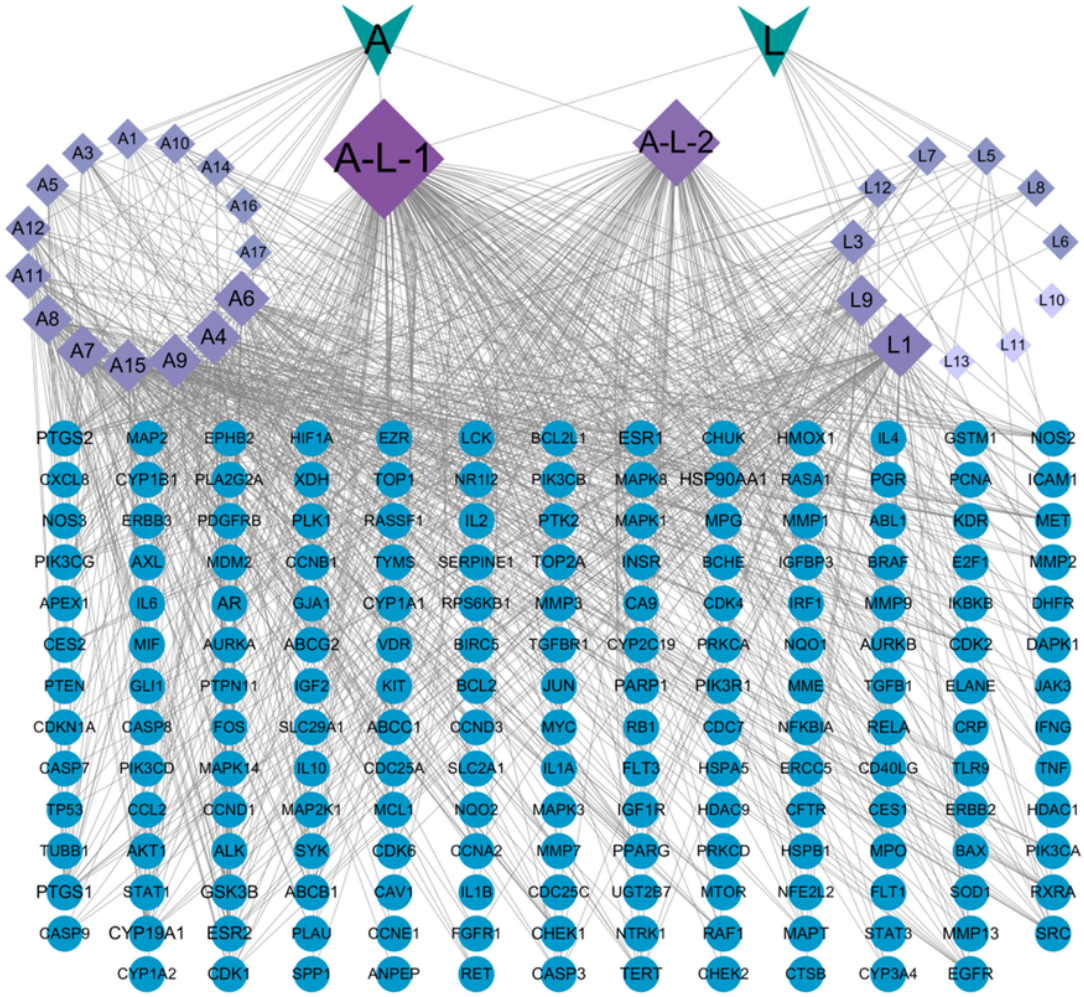


Figure 3

Bioactive compound–target network of "Astragalus-Ligustrum " drug pair

Green nodes: A represents *Astragalus*, L represents Ligustrum lucidum; The purple node: active ingredient; A-L represents the common active ingredient of "Astragalus–Ligustrum " drug pair; Blue nodes represent NSCLC targets

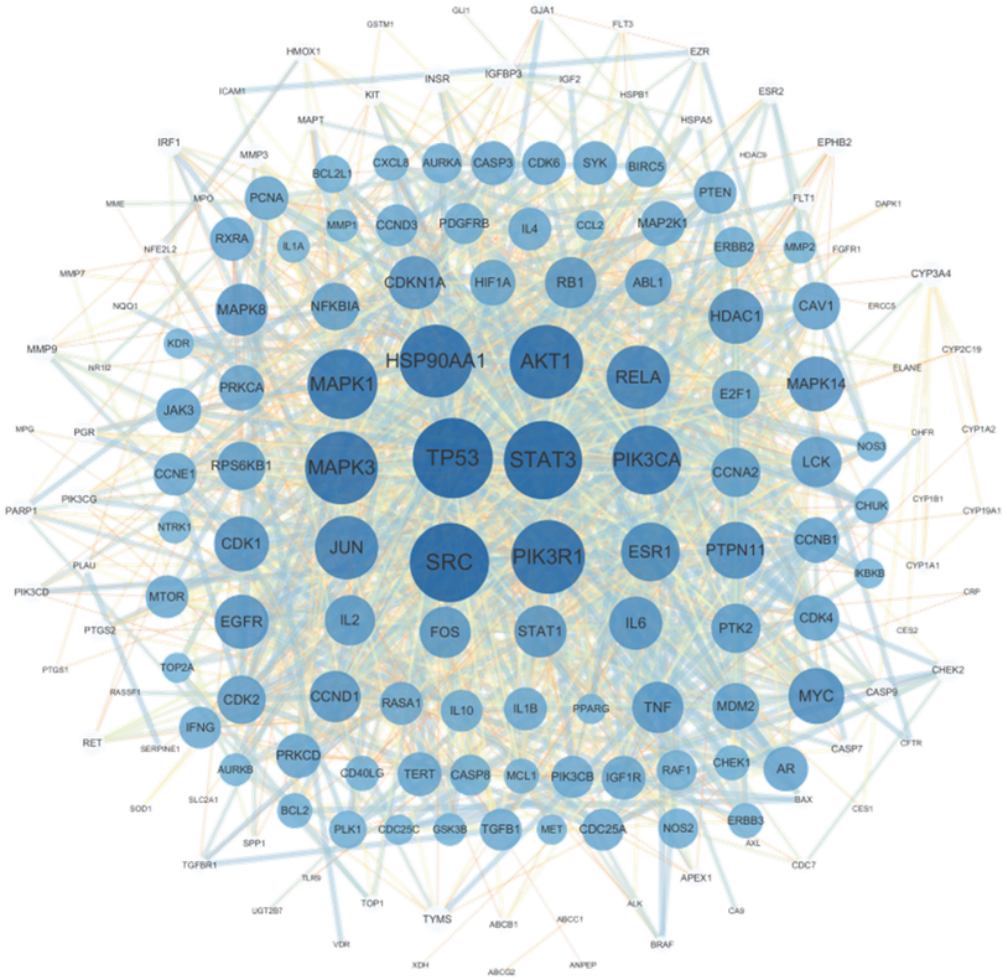


Figure 4

PPI network of "Astragalus–Ligustrum " combination in treatment of NSCLC

PPI:protein interactions; The magnitude of the degree value in the figure reflects the size of the node, and the color gradient is related to the betweenness centrality. The thickness of the edge and the gradient of the color are adjusted by the Edge betweennes and Combined score, respectively. The bigger the dot and the darker the color, the more of the protein is associated with other proteins in the whole network, and the more important it is.

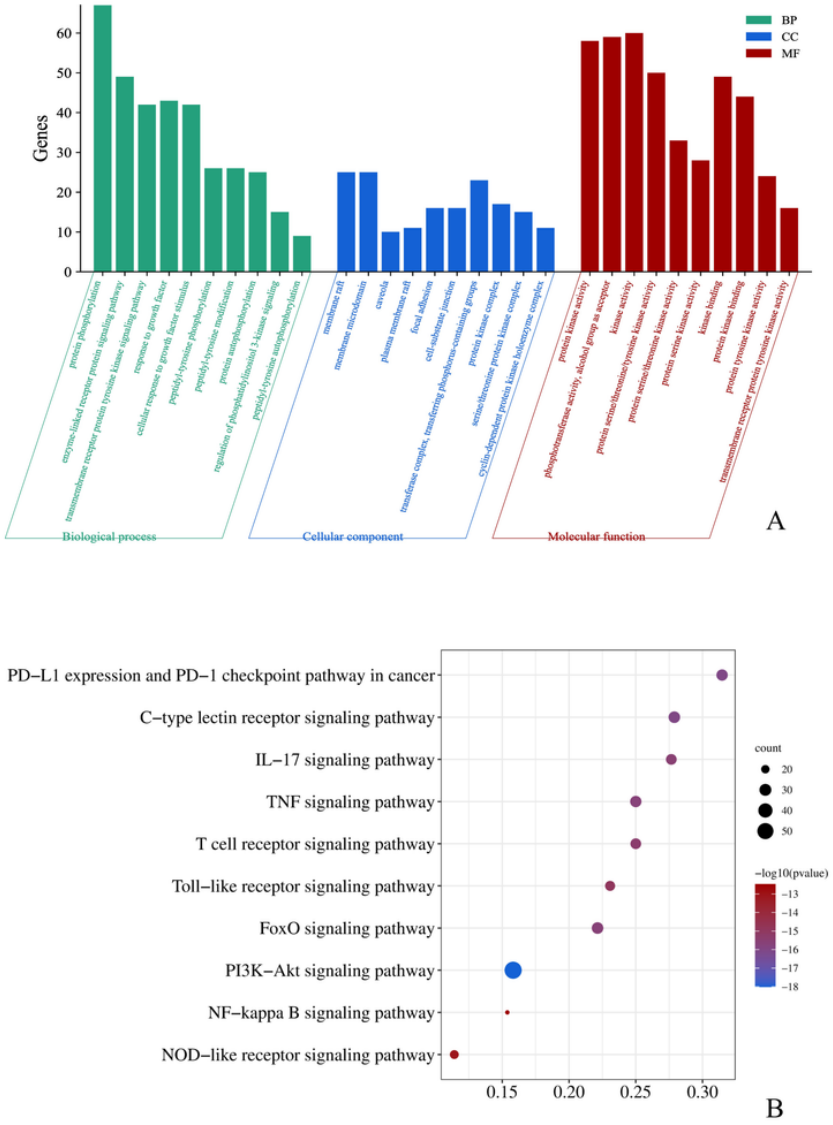


Figure 5

GO enrichment analysis and KEGG pathways enrichment analysis (a)GO enrichment analysis of “Astragalus–Ligustrum” drug pair in treatment of NSCLC; (b)KEGG pathways enrichment analysis of “Astragalus–Ligustrum” drug pair in treatment of NSCLC

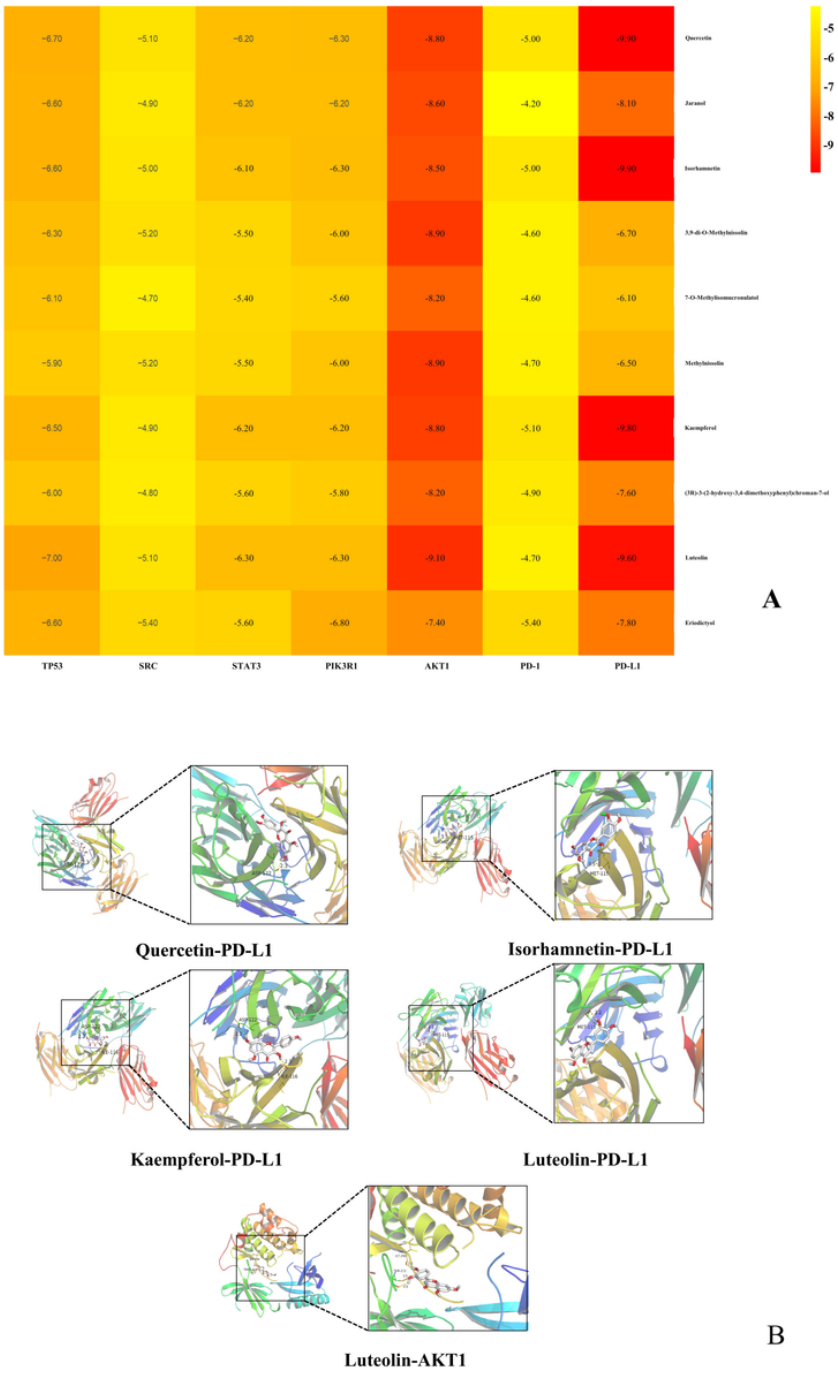


Figure 6

Prediction of binding energies and Docking conformations

(a)Prediction of binding energies of active ingredients and key targets in "Astragalus–Ligustrum "; The vertical axis represents the name of genes, and the horizontal axis represents the pathways. Each small block represents the signal intensity of a gene expression in a bin, the darker the color, the stronger the signal intensity.

(b)Docking conformations of Quercetin, Kaempferol, Isorhamnetin and Luteolin with PD–L1 or AKT1

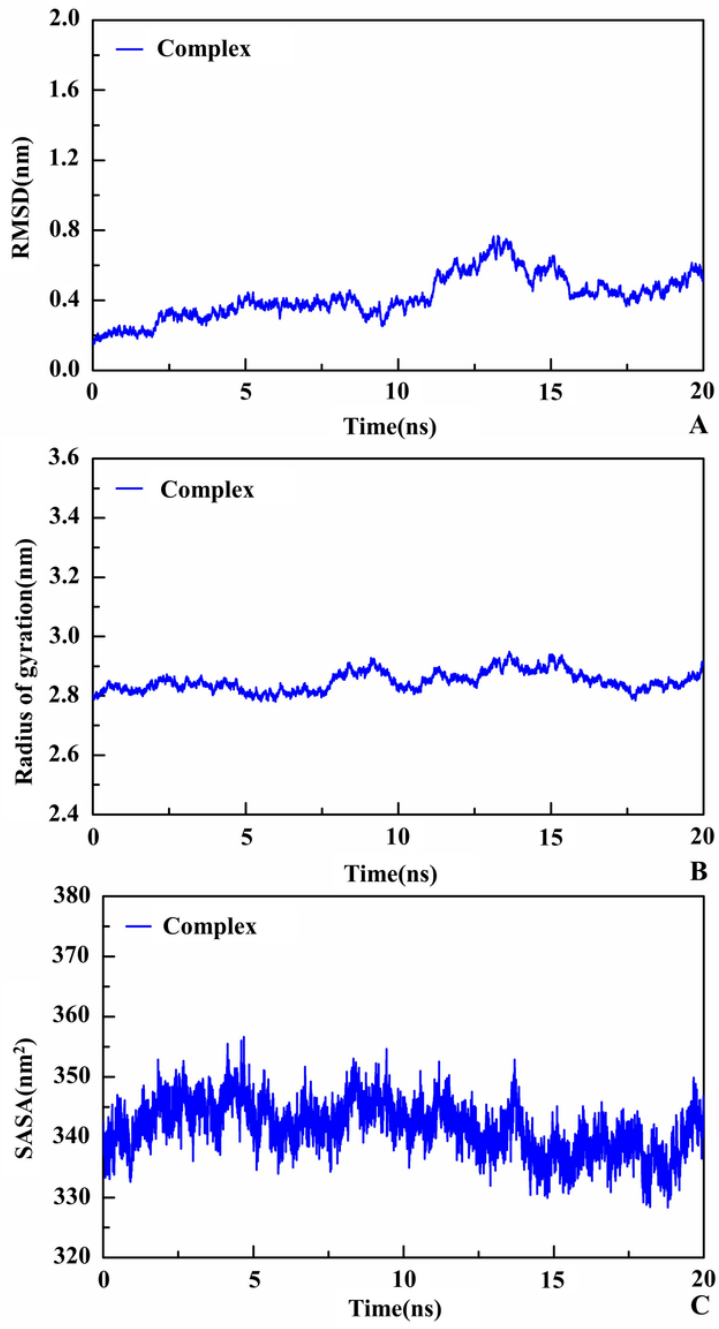


Figure 7

Analysis of RMSD, RMSF, Rg, and SASA of the complex

(a) Changes of RMSD over simulation time; The vertical axis represents the changes of RMSD, and the horizontal axis represents the change of time; (b) Changes of Rg over simulation time; The vertical axis represents the changes of Rg, and the horizontal axis represents the change of time; (c) Changes of SASA over simulation time; The vertical axis represents the changes of SASA, and the horizontal axis represents the change of time

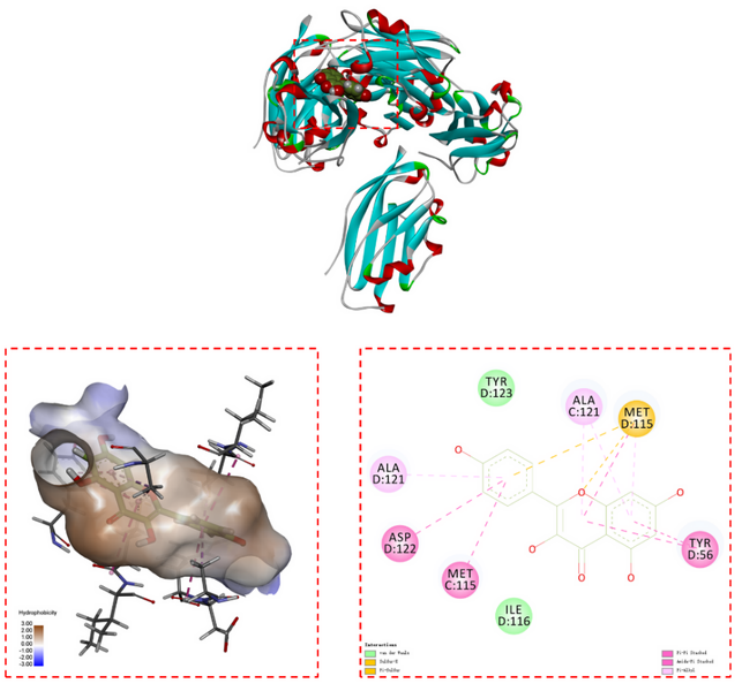


Figure 8

Combined mode diagram of small molecules and protein

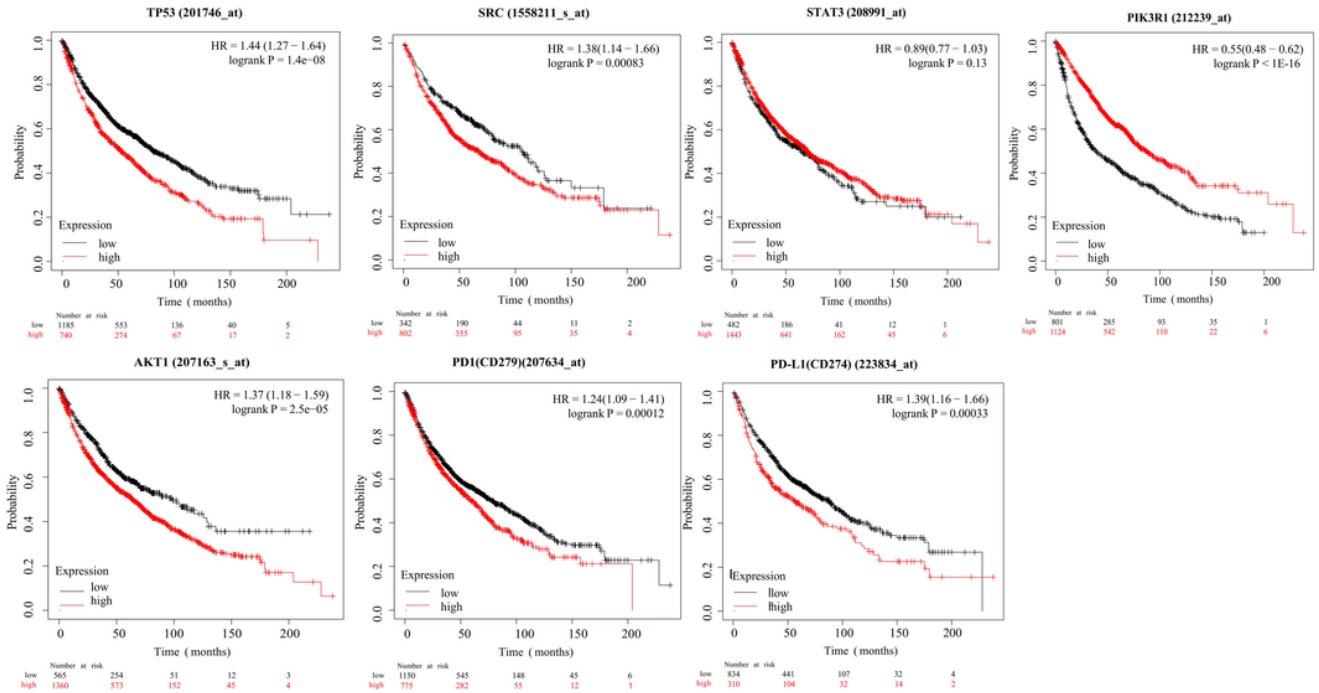


Figure 9

Survival curve and Protein expression of key targets in NSCLC or normal lung tissue

The vertical axis represents the survival rate, and the horizontal axis represents the observation time.

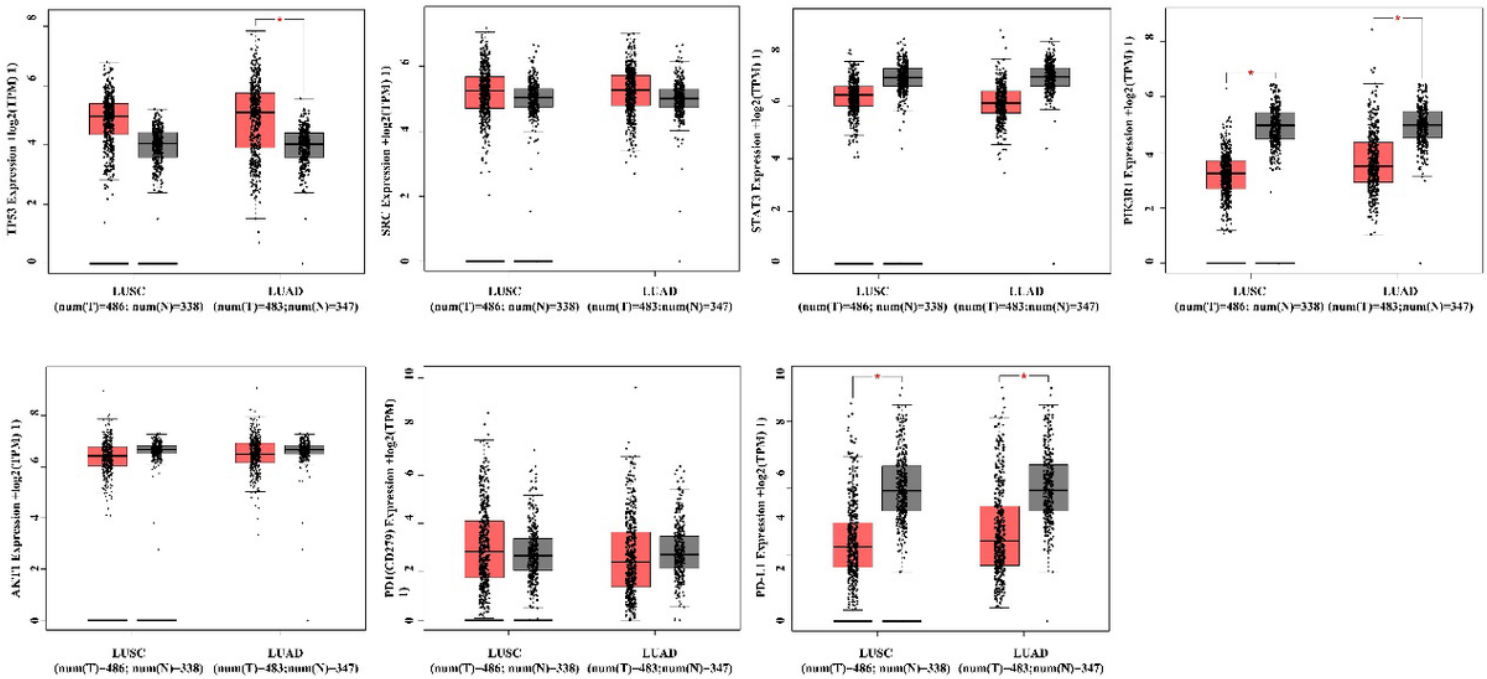


Figure 10

Gene expression in LUAD, LUSC and normal lung tissue

LUAD: lung adenocarcinoma; LUSC: lung squamous cell carcinoma

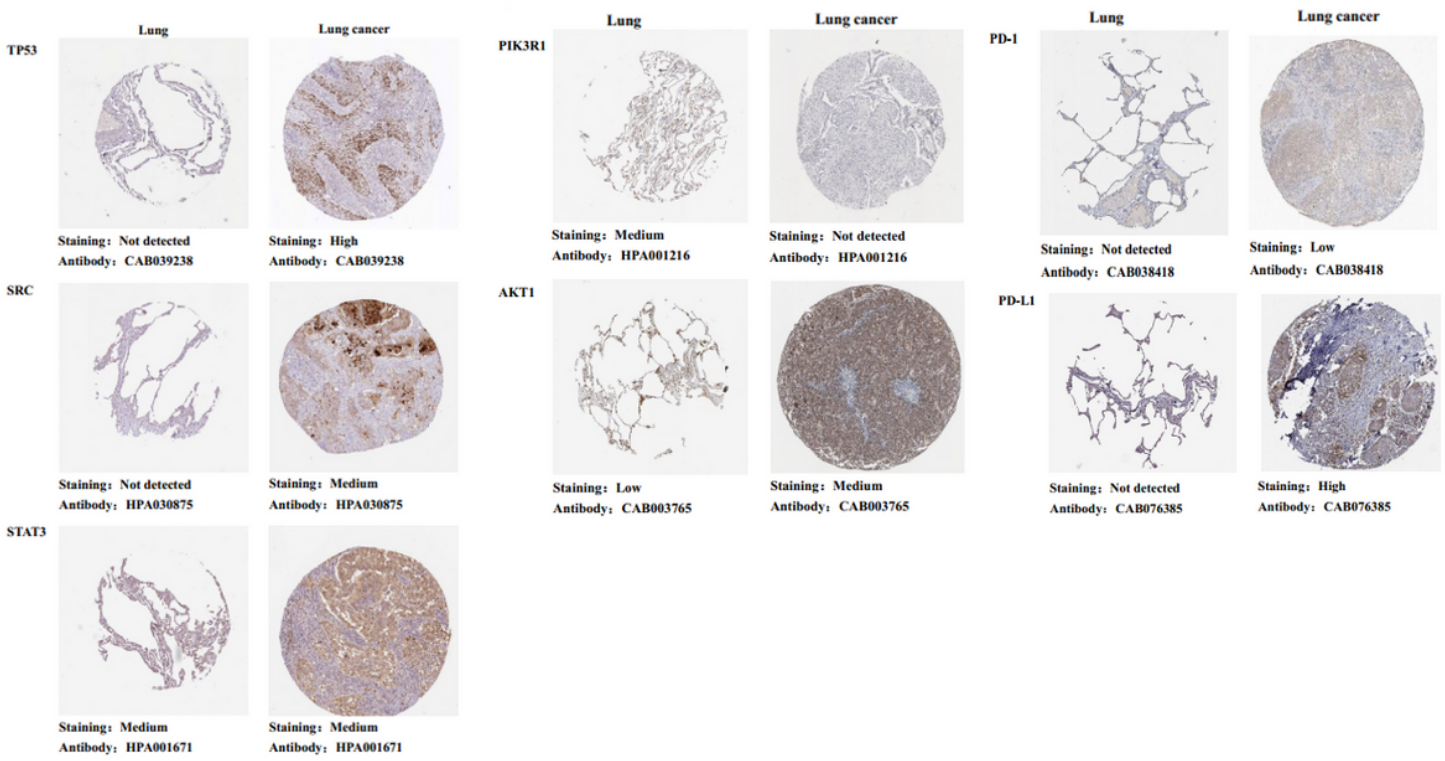


Figure 11

Protein expression levels of key targets in normal lung tissue and lung cancer tissue